Micro-scale truss structures with three-fold and six-fold symmetry formed from self-propagating polymer waveguides

Alan J. Jacobsen[1/2,*], William Barvosa-Carter[1], Steven Nutt[3]

1. HRL Laboratories LLC, Sensors and Materials Laboratory, 3011 Malibu Canyon Road, Malibu, CA 90265-4797, USA
2. Department of Aerospace and Mechanical Engineering, University of Southern California, Los Angeles, CA, USA
3. Department of Chemical Engineering and Materials Science, University of Southern California, Los Angeles, CA, USA

Abstract: A process for interconnecting a three-dimensional pattern of self-propagating polymer waveguides was used to form micro-truss structures with two new unit cell architectures. The structures were formed using a two-dimensional mask with a hexagonal pattern of apertures. Distinct unit cell architectures were possible by exposing the mask to a different number of incident UV exposure beams, which are used to form the waveguides. One unit cell design featured three intersecting waveguides per node, resulting in a structure with three-fold symmetry. The second unit cell design had six-fold symmetry and was characterized by primary nodes with six intersecting waveguides and secondary nodes with two intersecting waveguides. Compression loading experiments were conducted on micro-truss samples with comparable relative density values ($\rho/\rho s$ = 6.5%), but different unit cell architectures. The addition of secondary nodes in the structures based on the second design led to an increase in compressive modulus of up to 70% and an average increase in peak strength of 42%. The increase in compressive strength and modulus was attributed to a reduction in the truss-member slenderness ratio achieved through increased waveguide connectivity.

Key words: Mechanical properties; Cellular solids; Photo-polymer waveguides; Lithography; Rapid prototyping

*Corresponding author. HRL Laboratories LLC, Sensors and Materials Laboratory, 3011 Malibu Canyon Road, Malibu, CA 90265-4797, E-mail address: ajjacobsen@hrl.com (A.J. Jacobsen).

Please cite this article as: Naify, Christina J. and Chang, Chia-Ming and McKnight, Geoffrey and Scheulen, Florian and Nutt, Steven, **Membrane-type metamaterials: Transmission loss of multi-celled arrays** Journal of Applied Physics, 109, 104902 (2011), DOI:http://dx.doi.org/10.1063/1.3583656

1. Introduction

The mechanical properties of cellular materials depend strongly on the architecture and physical distribution of the solid material from which the cellular structure is comprised. Open-cellular materials with a random architecture, such as polymer foams, have been shown to exhibit bending-dominated behavior in the cell struts during elastic loading [1]. To increase the modulus and strength of cellular solids, three-dimensional open-cellular truss structures have been proposed [2], with the majority of research focusing on metallic lattice materials [3], [4], [5], [6] and [7]. The architecture of these ordered metallic structures enables the truss members, or struts, to stretch or compress during elastic loading. By changing the mode of deformation from bending-dominated to stretch/compress-dominated within the cellular structure, significant improvements in the modulus and strength can be achieved, particularly for ultra-low-density structures (relative density <10%) [1] and [8].

The metallic truss topologies studied to date stem from the available fabrication techniques, which include investment casting, perforated metal sheet forming, and wire or hollow tube lay-up [3] and [8]. Some of the unit cell configurations that can be produced by these fabrication techniques include tetrahedral [9], pyramidal [10], and three-dimensional Kagome structures. Hyun et al. [11] used finite-element simulations to show that the three-dimensional Kagome architecture was superior to the tetrahedral-based structures under compression and shear loading. Wang et al. [12] verified these results experimentally, concluding that the three-dimensional Kagome architecture outperformed both the tetrahedral and pyramidal-based truss structures.

Although the general three-dimensional Kagome structure has been shown to be mechanically efficient, fabrication techniques for these or similar structures have been limited until recently. The

Please cite this article as: Naify, Christina J. and Chang, Chia-Ming and McKnight, Geoffrey and Scheulen, Florian and Nutt, Steven, **Membrane-type metamaterials: Transmission loss of multi-celled arrays** Journal of Applied Physics, 109, 104902 (2011), DOI:http://dx.doi.org/10.1063/1.3583656

authors have developed a technique that can be used to create highly ordered open-cellular truss topologies from an interconnected pattern of self-propagating polymer waveguides [13]. This technique was recently used to create three-dimensional octahedral-type unit cell architectures from a two-dimensional mask with a square pattern of apertures [13]. The resulting open-cellular polymer materials featured micro-scale truss members and nodes and suppressed bending-dominated behavior under compression [14] and shear [15] loading. In the present work, we utilize a mask with a hexagonal pattern of apertures to create two distinct unit cell architectures with three-fold and six-fold symmetry. These cellular structures were tested under compression to investigate the effect of waveguide connectivity on the mechanical performance and failure modes.

2. Polymer micro-truss fabrication with hexagonal mask pattern

A polymer waveguide can be formed within a photosensitive monomer from a single point exposure of light [16], [17], [18] and [19]. By exposing a volume of photomonomer to multiple, angled collimated UV light beams through a mask with a two-dimensional pattern of apertures, multiple self-propagating waveguides originate from each aperture. The number of waveguides formed at each aperture and the direction and angle of these waveguides depend on the number of collimated exposure beams and the angle and direction of the beams at the mask surface. The waveguides naturally intersect during the formation process, so if a two-dimensional exposure surface is patterned appropriately, it produces an ordered three-dimensional open-cellular architecture. A schematic representation of this process is shown in Fig. 1a. Previous work describing cellular materials formed from this process utilized a mask with a square pattern of circular apertures to create a repeating octahedral-type unit cell [13] and [14]. By substituting a mask with a hexagonal

pattern of apertures (Fig. 1b), new architectures with three-fold and six-fold symmetry can be created.

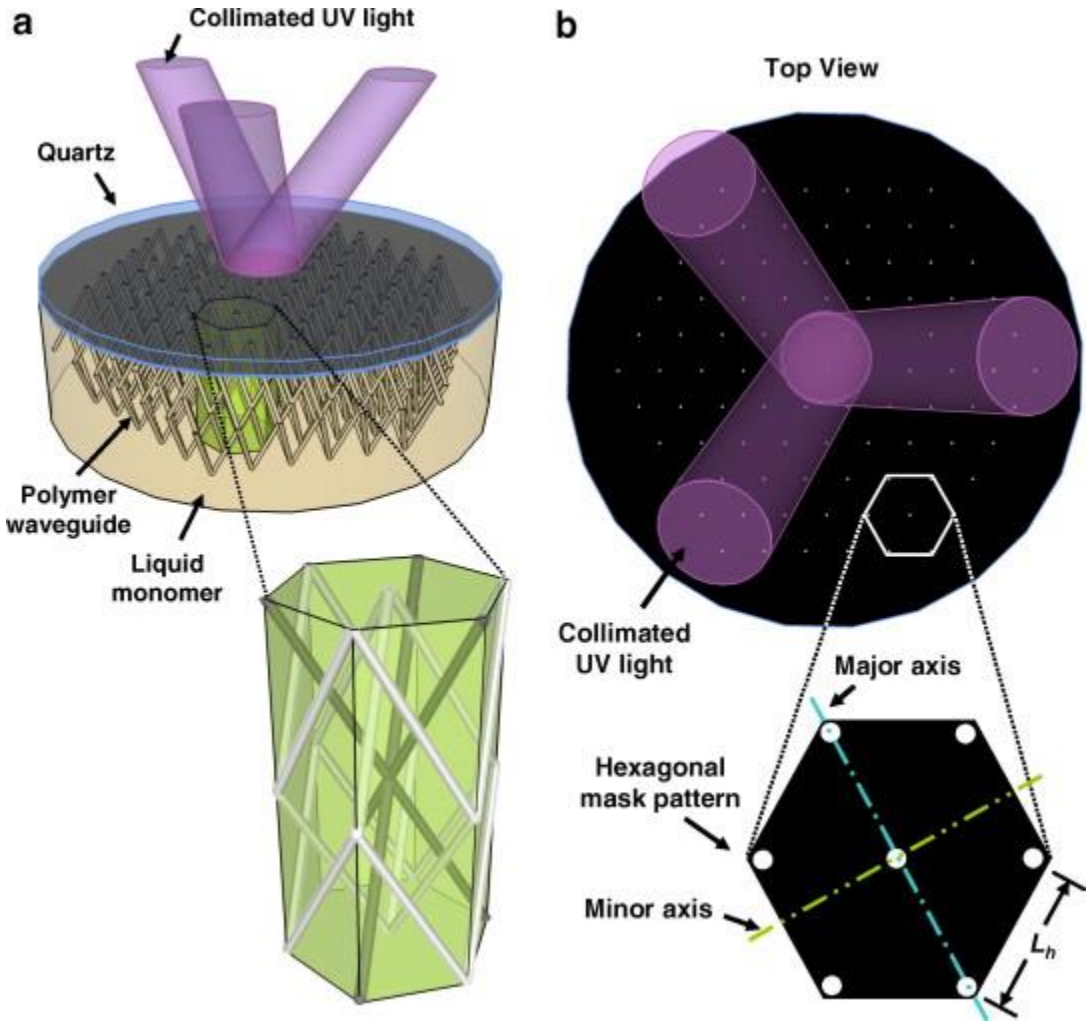

Fig. 1. *(a) Schematic of the set-up for creating micro-truss structures with an interconnected array of self-propagating waveguides and (b) the top view of the mask with a hexagonal pattern of circular apertures.*

2.1 Unit cell architecture

Two of the unit cell structures that can be created using a hexagonal mask pattern are shown in Fig. 2. Fig. 2a is a unit cell formed from three equally angled exposure beams, where each beam is aligned along the major axis of the hex pattern (see Fig. 1b) but rotated 120° apart with respect to the mask normal. The tetrahedral architecture of the waveguides in this unit cell will form the highlighted cell

in Fig. 1a if the structure is two unit cells thick. Fig. 2b is the unit cell that is formed if six angled exposure beams are used. Each of these beams is also aligned with a major axis of the hex pattern but rotated 60° with respect to the mask normal. Notice that the formation of six self-propagating waveguides from each aperture on the mask surface leads to a three-dimensional structure with increased waveguide connectivity within the described unit cell volume. This unit cell structure comprises two types of intersecting nodes: primary and secondary nodes. The primary nodes are formed from six intersecting waveguides and the secondary nodes are created from the intersection of two waveguides. The secondary nodes are located at the midpoint of each waveguide connecting adjacent primary nodes. Micrographs of cellular structures formed with these unit cell architectures are shown in Fig. 3.

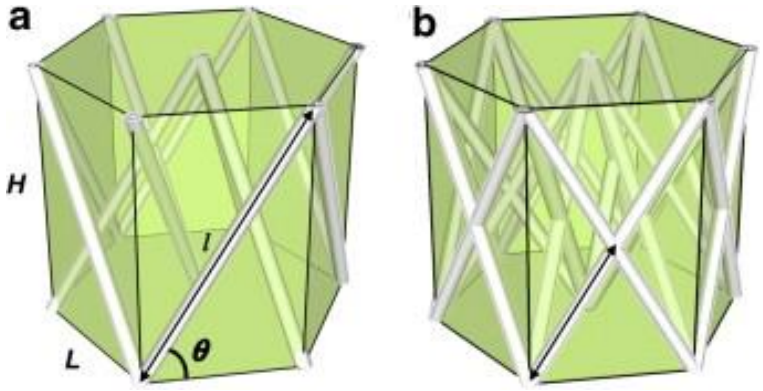

Fig. 2. *The two unit cell architectures that were formed using the mask with apertures in a hexagonal pattern. (a) The unit cell formed with three incident UV exposure beams and (b) the unit cell formed with six exposure beams.*

Please cite this article as: Naify, Christina J. and Chang, Chia-Ming and McKnight, Geoffrey and Scheulen, Florian and Nutt, Steven, **Membrane-type metamaterials: Transmission loss of multi-celled arrays** Journal of Applied Physics, 109, 104902 (2011), DOI:http://dx.doi.org/10.1063/1.3583656

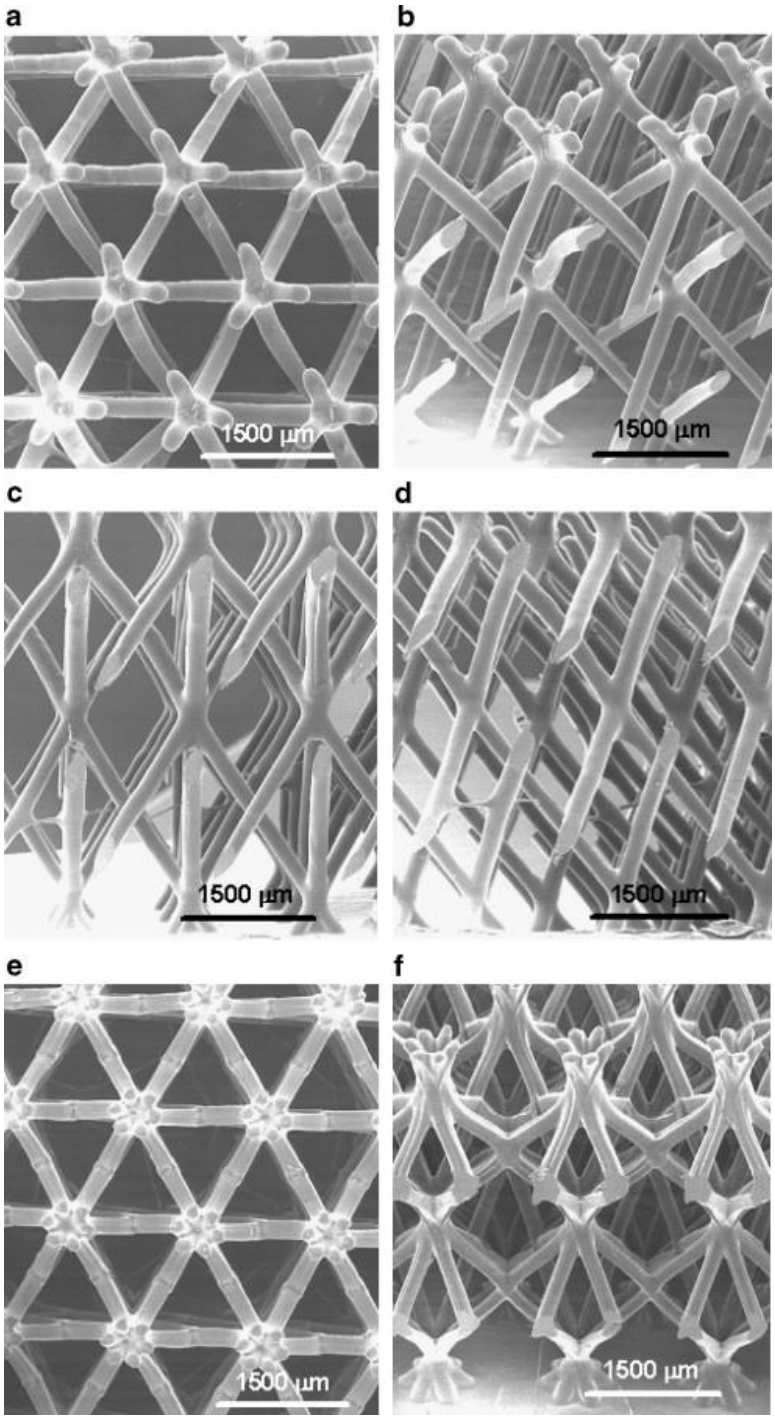

Fig. 3*. (a) Top view, (b) perspective view, and (c–d) side views of the polymer micro-truss structures formed with three UV exposure beams. (e) Top view and (f) perspective view of the unit cell with six-fold symmetry.*

2.2 Relative Density

Relative density is defined as the density of a cellular material (ρ) divided by the density of the solid material (ρ_s) from which it is comprised. By definition, it is also a measure of the solid volume fraction of a cellular material, which can be determined from the geometric parameters of the repeating unit cell, such as waveguide radius (r), length (l), and angle (θ). An equation used to estimate the relative density for a structure with three-fold symmetry (Fig. 2a) is given below.

$$\left(\frac{\rho}{\rho_s}\right)_{3n} = \frac{9\pi r^2\sqrt{L^2+H^2}}{\left(\frac{3\sqrt{3}}{2}\right)L^2H} = \left(\frac{2\sqrt{3}\pi}{\cos^2\theta\sin\theta}\right)\left(\frac{r}{l}\right)^2_{3n} \quad (1)$$

The structures with six-fold symmetry have twice the number of waveguides per unit cell and increased waveguide connectivity. Taking into account the reduced truss member length ($l_{6n} = 0.5\ l_{3n}$) between nodes, the relative density for this unit cell architecture can be calculated from the following equation.

$$\left(\frac{\rho}{\rho_s}\right)_{6n} = \left(\frac{\sqrt{3}\pi}{\cos^2\theta\sin\theta}\right)\left(\frac{r}{l}\right)^2_{6n} \quad (2)$$

In previous studies, a square mask pattern was used to fabricate micro-truss structures with an octahedral-type unit cell [14]. An equation similar to Eqs. (1) and (2) was derived to determine the relative density based on the geometric parameters of this unit cell. Assuming an equal relative density and truss member angle θ, a relationship between the slenderness ratios for the octahedral-type unit cell $(l/r)_{4n}$ and the hex-based unit cell with six intersecting waveguides can be derived.

$$\left(\frac{\sqrt{3}\pi}{\cos^2\theta\sin\theta}\right)\left(\frac{r}{l}\right)^2_{6n} = \left(\frac{2\pi}{\cos^2\theta\sin\theta}\right)\left(\frac{r}{l}\right)^2_{4n} \quad (3)$$

$$\left(\frac{l}{r}\right)_{6n} = 0.93\left(\frac{l}{r}\right)_{4n} \quad (4)$$

This relationship indicates that for an equivalent relative density and truss member angle, the slenderness ratio of the truss members in the unit cell shown in Fig. 2b is slightly less that the octahedral-type unit cell. In addition, the unit cells considered in this work should exhibit greater isotropy in shear [12].

3. Prediction of compressive modulus and peak strength

The compressive modulus of an open-cellular material (E) that exhibits compression-dominated behavior in the struts during elastic loading can be predicted from the following expression [20] and [21],

$$E = E_s \sin^4\theta(\rho/\rho_s) \quad (5)$$

where E_s is the modulus of the solid material. The stress in each solid truss member (σ_s) can be calculated from the compressive stress applied to the cellular material (σ), the waveguide angle, and the relative density [21].

$$\sigma_s = \frac{\sigma}{\sin^2\theta(\rho/\rho_s)} \quad (6)$$

Alternatively, the peak stress of the bulk cellular material can be predicted from Eq. (6), assuming the maximum compressive stress that can be sustained in the truss members before buckling, yielding, or fracture is known. The truss member failure stress under ideal conditions can be predicted as a function of slenderness ratio (l/r), as shown in Fig. 4 [14]. Truss members with small slenderness ratios (<5) will fail by material yielding. As the slenderness ratio is increased, failure will transition from material yielding to inelastic buckling and eventually Euler buckling [22].

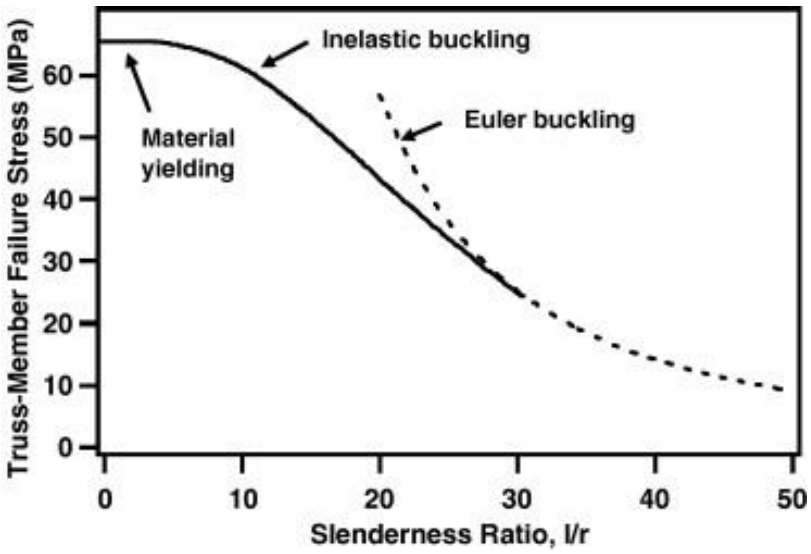

Fig. 4*. The predicted truss-member failure stress as a function of slenderness ratio for the photopolymer used to form the micro-truss structures [14].*

If the number of load bearing truss members in a unit cell volume is doubled and the angle of the truss members θ remains equal (as is the case from Fig. 2a and b), the radius of each truss member must be reduced by a factor of $1/\sqrt{2}$ to maintain a constant relative density. Thus, increasing the number of truss members without changing the relative density will not change the stress in each truss member, only the slenderness ratio. If secondary nodes are neglected, the slenderness ratio of the truss members will increase by a factor of $\sqrt{2}$, which in turn will decrease the maximum

theoretical failure stress of the cellular structure. However, the secondary nodes formed at *l*/2 in the structures with six-fold symmetry will decrease the slenderness ratio of each truss member by $1/\sqrt{2}$, thereby increasing the theoretical failure stress in comparison to the structures with three-fold symmetry.

If the waveguide overlap at the nodes is considered when the number of truss members in a unit cell volume is doubled, the actual reduction in waveguide radius necessary to maintain a constant relative density is less than a factor of $1/\sqrt{2}$. The mass that would occupy this overlapping region can be redistributed to increase the truss member radius, and thus decrease the stress in each truss member. This effect becomes more significant if the number of waveguides intersecting at each nodal region is further increased. However, increasing the number of waveguides that intersect at a node creates a stress concentration at that nodal region, which may cause material yielding at the node prior to reaching the expected truss member failure stress.

In reality, these micro-truss structures have imperfections, such as waveguide misalignment, that will lower the actual truss member failure stress. Also, as a result of the formation process, the nodal regions can overcure and therefore thicken, reducing the stress concentration effect. Compression experiments were conducted on multiple micro-truss structures with the repeating unit cells shown in Fig. 2 to better understand these competing mechanisms.

4. Experimental

4.1 Parent material properties

All micro-truss samples were formed with a thiol-ene polymer system previously characterized [14]. The modulus of the solid polymer E_s is 2.4 GPa and the density ρ_s is 1.34 ± 0.01 g cm^{-3}.

4.2 Polymer micro-truss samples for compression loading

Six micro-truss samples were fabricated for compression testing using a hexagonal mask pattern, as described in Section 2. The aperture radius was 75 μm and the spacingL_h between adjacent apertures was 1731 μm. Three samples (Samples 1–3) were produced using three incident UV beams, resulting in a microstructure with the repeating unit cell shown in Fig. 2a. The remaining three samples (Samples 4–6) were produced with six incident UV beams to form micro-truss structures with the unit cell shown in Fig. 2b. Each collimated beam was generated from a mercury arc lamp with a fluence of ~7.5 mW cm^{-2} at the mask surface. The angle of each incident light beam off the mask substrate surface remained constant for all samples (~20°). Due to the index of refraction change between air, quartz, and the monomer, the resulting waveguide angle θ was approximately 51°.

The mold containing the liquid monomer during micro-truss fabrication was approximately 5 mm deep. During the formation process, the waveguides first propagate to the bottom surface of the mold, and increased exposure time causes each waveguide to thicken. Eventually, if exposure is continued, the entire volume of monomer will cure.

The exposure time for Samples 1–3 was 70s; significantly shorter exposure times did not yield a structure that was sufficiently self-supporting when removing the uncured monomer in toluene. This

Please cite this article as: Naify, Christina J. and Chang, Chia-Ming and McKnight, Geoffrey and Scheulen, Florian and Nutt, Steven, **Membrane-type metamaterials: Transmission loss of multi-celled arrays** Journal of Applied Physics, 109, 104902 (2011), DOI:http://dx.doi.org/10.1063/1.3583656

relatively long exposure time formed waveguides with a radius of approximately 120 μm. The exposure time for Samples 4–6 was 35 s, which was determined experimentally to yield micro-truss structures with a density approximately equal to Samples 1–3.

All samples were post-cured for 24 h at 130 °C under vacuum while still attached to the 1.5 mm thick quartz plate that separated the mask and monomer. After post-cure, each sample was cut into the shape of a hexagon with a razor blade. The surface area dimensions and thickness were measured within ±0.1 mm using digital calipers. The mass of each sample attached to the quartz plate was measured on a scale with 0.001 g accuracy. The mass of each quartz plate was measured prior to sample fabrication, and subtracted to determine the mass of each sample.

Samples 1–3 had a hexagonal "footprint" with 12 unit cells per edge (~20 mm). Samples 4, 5 and 6 were cut in hexagonal shapes with 9, 10 and 11 unit cells per edge, respectively, to determine if edge effects played a significant role on the compression properties of samples this size. The measured micro-truss parameters for all samples tested under compression are summarized in Table 1. As discussed in previous work, the small variation in density between similar samples was attributed to sensitivities in the process [14].

Table 1. *Summary of the measured parameters for the micro-truss structures tested under compression*

Sample	Micro-truss parameters							
	No. of incident UV light beams	Density ρ (g cm^{-3})	Measured relative density ρ/ρ_s (%)	Calculated relative density[a] ρ/ρ_s(%)	Waveguide length/ (mm)	Waveguide radius r (μm)	Waveguide angle[b] θ(deg)	No. of Unit cells/ edge
1	3	0.081	6.1	6.5	2.8	120 ± 5	51 ± 1	12
2	3	0.087	6.5	6.5	2.8	120 ± 5	51 ± 1	12
3	3	0.090	6.7	6.5	2.8	120 ± 5	51 ± 1	12
4	6	0.087	6.5	7.3	2.8	90 ± 5	51 ± 2	9
5	6	0.085	6.3	7.3	2.8	90 ± 5	51 ± 2	10
6	6	0.086	6.4	7.3	2.8	90 ± 5	51 ± 2	11

[a]*Relative density calculated using Eqs. (1) and (2).*

[b]*Waveguide angle measured relative to initiating substrate surface.*

To constrain the nodes at the waveguide terminating surface of each sample during compression, an additional quartz plate was attached to the open surface of the structures with a thin layer of the same photopolymer used to fabricate the structures. A compression sample with six-fold symmetry sandwiched between two quartz plates is shown in Fig. 5.

Fig. 5. *Image of a polymer micro-truss sample sandwiched between two quartz plates.*

4.3 Compression experiments

The six samples described in the previous section were subjected to compressive loading using a hydraulic load frame and a constant strain rate of 2×10^{-3} s^{-1}. The displacement was measured using a laser extensometer with 0.001 mm precision. The applied force was measured using a load cell with an accuracy of ±1%. The accuracy of all reported compression stress data is ±2%.

5. Results and discussion

All six samples exhibited a linear elastic region during the initial stage of compression. As the compressive strain increased, the stress increased until the truss members buckled, after which there was a marked decrease in stress. The stress reached a minimum at approximately 20% strain for each sample and then gradually increased until the strain reached approximately 60%, at which point densification led to a rapid increase in stress.Fig. 6 is the nominal compressive stress–strain data for two samples (Samples 2 and 4) of equal measured relative density, but different unit cell architectures. The increase in peak strength and modulus of Sample 4 is attributed to the reduced slenderness ratio in the six-fold symmetric structure, as discussed in the following sections.

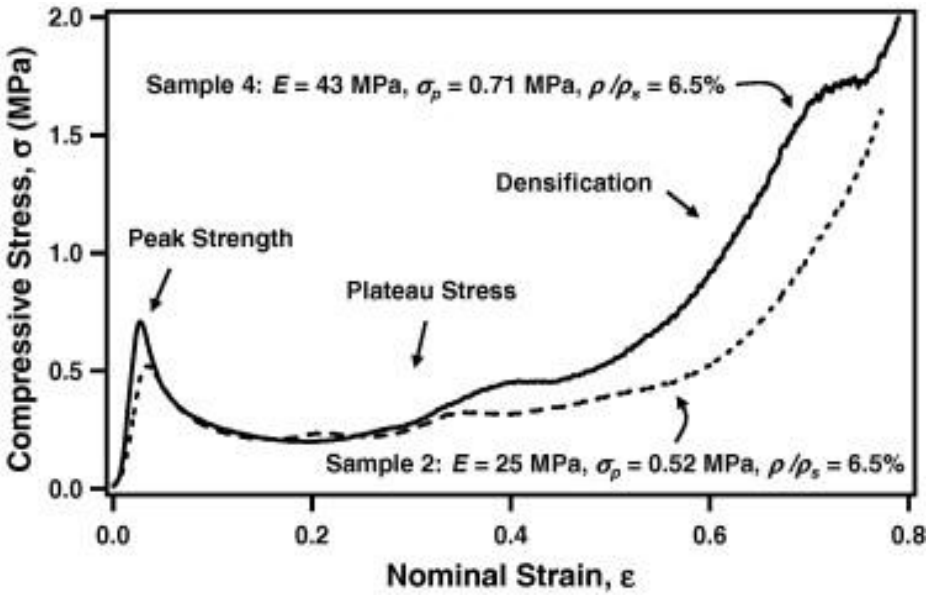

Fig. 6. *A comparison of the compressive response for the two different unit cell architectures.*

5.1 Compressive modulus

The compressive modulus *E* for the micro-truss samples was determined from the average slope of the nominal stress–strain curve. The average slope was measured between 25% and 75% of the respective peak stress values to avoid the nonlinear behavior arising from preloading affects at low stresses and the onset of buckling at higher stress levels. The measured compressive moduli are shown in Table 2. The difference in the measured compressive moduli of the samples with three-fold and six-fold symmetry is a result of different dominating imperfections for each unit cell architecture.

***Table 2**. Summary of the measured compressive properties*

Sample	Compressive modulus (MPa)	Peak strength (MPa)	Average peak truss member stress (MPa)
1	35 ± 0.2	0.48	13.0
2	25 ± 0.2	0.52	13.2
3	31 ± 0.2	0.54	13.3
4	43 ± 0.3	0.71	18.1
5	42 ± 0.2	0.76	20.0
6	43 ± 0.4	0.74	19.1

The modulus values for the samples with three-fold symmetry (Samples 1–3) varied significantly (up to 40%). From Eq. (5), the predicted modulus for a micro-truss sample with waveguides at $\theta = 51°$ and a relative density of 6.5% is 57 MPa, while the measured values range between 25 and 35 MPa. The discrepancy in measured and predicted values, along with the inconsistency of the measured modulus values, is attributed to the long slenderness ratio of the truss members ($l/r > 20$) coupled with inherent imperfections. As l/r is increased, the truss members are more susceptible to bend during elastic compressive loading. The degree to which the truss members bend prior to buckling will significantly affect the modulus of the micro-truss material [1].

The samples with six-fold symmetry exhibited consistent measured modulus values. However, these values were approximately 33% less than the modulus values predicted from Eq. (5). Closer examination of the microstructure revealed the waveguide angle θdecreased through the sample thickness in structures produced with this unit cell architecture. Although the incident angle of UV light was constant for all samples in this study, the thinner truss members in Samples 4–6 led to structural relaxation during subsequent processing steps, which caused cell-to-cell angle variations through the thickness of the micro-truss. Fig. 7a and b clearly show the difference in waveguide angle between the unit cell adjacent to the initiating substrate (7a) and the unit cell at the terminating

surface of the waveguides (7b). An additional indication of relaxation appeared in the measured thickness of Samples 4–6, which was an average of 4% less than the thickness of Samples 1–3.

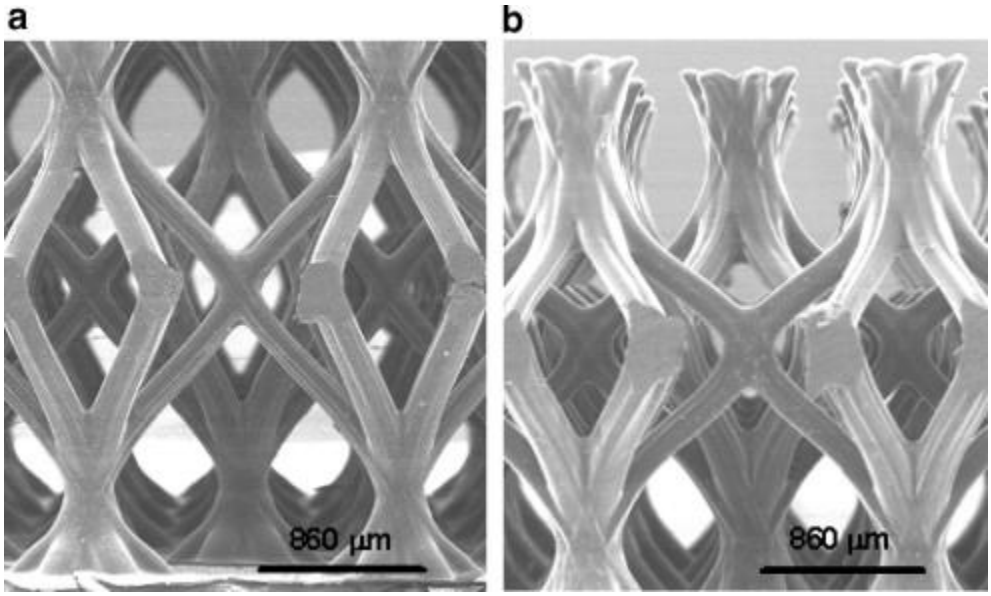

Fig. 7. *A representative unit cell (a) adjacent to the initiating substrate surface and (b) adjacent to the waveguide terminating surface for the structures with six-fold symmetry. These SEM images show the change in waveguide angle through the thickness of the micro-truss structure due to relaxation during processing.*

From Eq. (5), the modulus scales with $\sin^4 \theta$ and thus is sensitive to variations in waveguide angle. This was verified in previous work where micro-truss structures with different waveguide angles were tested under compressive loading [14]. The change in truss member angle through the thickness accounts for the difference between the measured and predicted moduli. For example, if an average angle of $\theta = 46°$ is used in Eq. (5), the predicted modulus for a micro-truss with a relative density of 6.5% is 42 MPa (compared with 57 MPa when $\theta = 51°$).

Comparing the measured modulus values for samples with equal relative density but differing architectures illustrates the effect of suppressing bending during elastic loading. Increasing the connectivity of the waveguides (as in the unit cell shown in Fig. 2b) reduced the effective slenderness ratio of the truss members, thus decreasing the susceptibility to bending. Although the structures with six-fold symmetry had a significantly reduced waveguide angle due to relaxation, the measured modulus was still 20–70% greater than the alternative unit cell structure.

5.2 Peak strength

Authors The peak strength for the polymer micro-truss materials is defined as the maximum stress prior to initial buckling failure. The measured peak strength for each sample is listed in Table 2. SEM images of representative samples deformed just beyond plastic buckling of the waveguides (approximately 20% strain) are shown in Fig. 8. Prior to imaging in the SEM, the samples were cut with a wafering saw to expose the interior of the sample after buckling.

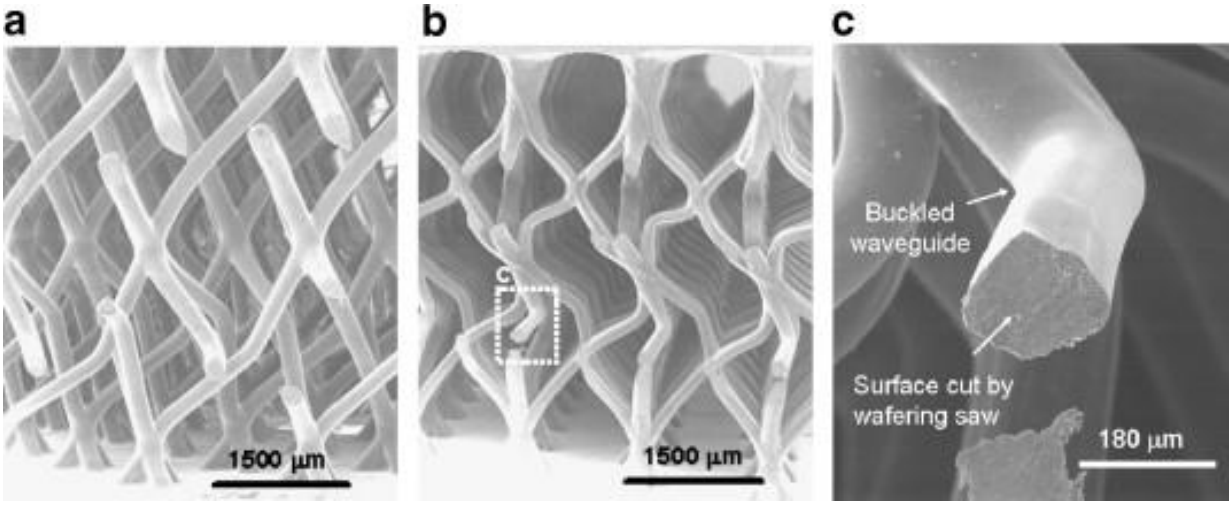

Fig. 8. *(a) A structure with three-fold symmetry and (b) a structure with six-fold symmetry compressed just beyond the point of initial truss member buckling. (c) A close-up image of a buckled truss member in (b).*

The estimated stress in a single truss member at the peak strength of each sample was calculated using Eq. (6), and these values are tabulated in Table 2. When the slenderness ratio of the truss members in the unit cell was decreased, the average peak strength increased by over 40%. However, the maximum stress in each truss member was still less than the theoretical buckling stress for ideal loading conditions, as indicated in Fig. 4.

For both unit cell architectures, the measured peak stress was repeatable. This was expected for Samples 4–6, which exhibited similar elastic response in compression. However, based on the variation in modulus between Samples 1–3, the repeatability in the peak strength of these samples was surprising. Based on the measured cross-sectional area of the nodal regions, the maximum compressive stress at each node was calculated to determine if the yield stress was exceeded. The nodes in Samples 1–3 and Samples 4–6 experienced a maximum stress of approximately 28 MPa and 47 MPa, respectively, which are well below the measured yield strength of the bulk polymer (65 MPa, see Fig. 4).

One possible explanation for the results described above is that the measured modulus of structures with long-slenderness-ratio truss members is dominated by the initial curvature in the waveguides, and the peak strength is dominated by waveguide misalignment at the nodes. With fewer intersecting waveguides at each node, nodal stability presumably decreases, leading to rotations that initiate buckling at lower stress levels. These results require further investigation of the role of imperfections in these micro-truss structures.

5.3 Sample size effect

Authors For all samples, the unit cell size was relatively large in comparison to the overall bulk sample dimensions. Therefore, Samples 4–6 were cut to different sizes to determine if edge effects played a significant role in the measured compressive response. Sample 4 had a total of 9 unit cells per edge, while Sample 5 had one additional unit cell per edge, and Sample 6 had two additional unit cells per edge. The stress–strain response for these three samples, shown in Fig. 9, was repeatable and thus edge effects were not observable in these samples.

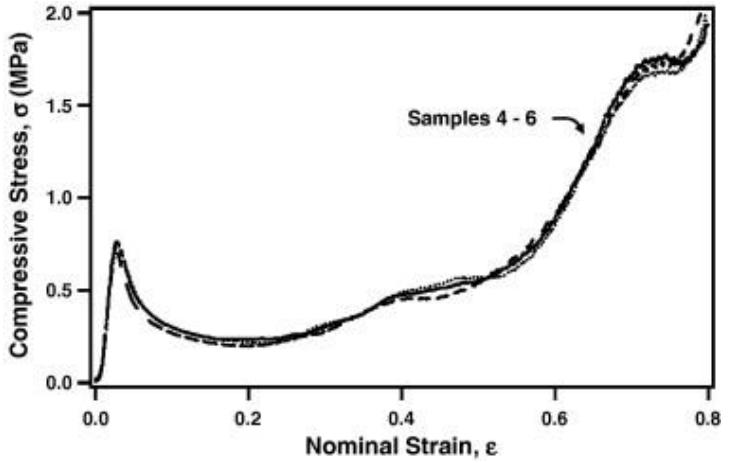

Fig. 9. *The compressive stress–strain curve for samples with six-fold symmetry is repeatable for samples with 9, 10, and 11 unit cells per sample edge.*

5.4 Comparison between unit cell structures

Although theoretically the slenderness ratio should only affect the peak strength and not the modulus, we have shown that long-slenderness-ratio waveguides are more susceptible to non-ideal bending deformation during compressive loading. Thus, unit cell architectures with the shortest slenderness ratio for a given relative density result in higher strength and stiffness values.

In Fig. 10, the specific compressive behavior of Samples 2 and 4 is compared to the behavior of a sample with a repeating octahedral-type unit cell and approximately equal truss member angle [14]. The measured compressive stress was normalized by the density of each structure since Samples 2 and 4 were approximately half the density of the octahedral sample. Theoretically, Sample 4 should have greater specific peak strength than the micro-truss sample with the octahedral unit cell structure because the truss members of a six-fold symmetric unit-cell have a lower slenderness ratio. However, the increased susceptibility to non-ideal deformation of the lower density structures (as in Sample 4) leads to a lower specific strength and modulus.

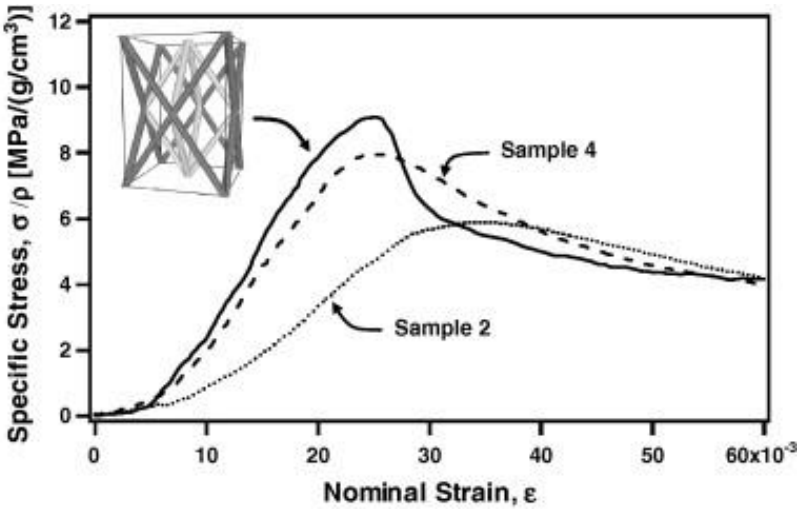

Fig. 10. *A comparison of the elastic and post-buckling response between the architectures in this study and an octahedral unit cell [14] with a similar truss member angle ($\theta \cong 51°$). The measured compressive stress was normalized by the density of each structure.*

Also, the octahedral-based structure exhibits a sharp decrease in stress after initial buckling. In contrast, the unit cells tested in this study display a softer transition to the plateau stress. This finding is similar to the compression behavior of three-dimensional Kagome architectures discussed in previous studies [11] and [12].

6. Conclusions

The process of interconnecting self-propagating polymer waveguides has been used to create micro-truss structures with three-fold and six-fold symmetric unit cells, and compression experiments were conducted on samples with these new architectures to understand their deformation behavior. The measured compression modulus of the structures with six-fold symmetry was approximately 20–70% greater than the modulus values for the structures produced with three-fold symmetry. The discrepancy in the measured and predicted moduli, as well as the inconsistency in the modulus of the three-fold-symmetric structures, was attributed to the difference in the truss member slenderness ratios between the competing architectures. The secondary nodes in the six-intersecting-waveguide structures reduced the slenderness ratio of the truss members without increasing the relative density. This reduced the structure's susceptibility to non-ideal deformation. The smaller slenderness ratio also increased the peak strength of the structures by an average of 42%, although these values were still below idealized predictions.

As demonstrated with this process, micro-truss structures with different architectures that are multiple unit cells thick can be fabricated from a single, two-dimensional exposure surface. These structures have unit cell features, such as waveguide diameter, on the order of tens to hundreds of microns. However, with improvements in the process, forming these structures with smaller diameter waveguides may be possible. This could ultimately lead to micro-truss structures with interesting mechanical properties introduced by size effects.

In addition to the two unit cell architectures presented in this work, the same or similar mask pattern could be used to create other unit cell configurations including non-symmetric structures. For

example, a non-symmetric exposure pattern could be used to create a micro-truss structure that preferentially deformed or failed in a specific manner, or masks with spatial variations in the aperture pattern could be used to create graded structures with unique mechanical and multifunctional properties.

Acknowledgements: One of the authors (A. J. Jacobsen) would like to thank the National Physical Science Consortium for fellowship support. Also, the authors thank Chaoyin Zhou and Bob Doty for their helpful discussions and technical assistance.

References:

1. Ashby MF. Phil Trans R Soc A 2006;364:15.
2. Deshpande VS, Ashby MF, Fleck NA. Acta Mater 2001;49:1035.
3. Wadley HNG. Phil Trans R Soc A 2006;364:31.
4. Wadley HNG, Fleck NA, Evans AG. Compos Sci Technol 2003;63:2331.
5. Queheillalt DT, Wadley HNG. Acta Mater 2005;53:303.
6. Wallach JC, Gibson LJ. Int J Solid Struct 2001;38:7181.
7. Wicks N, Hutchinson JW. Int J Solid Struct 2001;38:5165.
8. Wadley HNG. Adv Eng Mater 2002;4:726.
9. Kooistra GW, Deshpande VS, Wadley HNG. Acta Mater 2004;52:4229.
10. Zok FW, Waltner SA, Wei Z, Rathbun HJ, McMeeking RM, Evans AG. Int J Solid Struct 2004;41:6249.
11. Hyun S, Karlsson AM, Torquato S, Evans AG. Int J Solid Struct 2003;40:6989.
12. Wang J, Evans AG, Dharmasena K, Wadley HNG. Int J Solid Struct 2003;40:6981.
13. Jacobsen AJ, Barvosa-Carter W, Nutt S. Adv Mater 2007;19:3892.
14. Jacobsen AJ, Barvosa-Carter W, Nutt S. Acta Mater 2007;55:6724.
15. Jacobsen AJ, Barvosa-Carter W, Nutt S. Acta Mater 2008;56:1209.
16. Kewitsch AS, Yariv A. Appl Phys Lett 1996;68:455.
17. Kewitsch AS, Yariv A. Opt Lett 1996;21:24.
18. Kagami M, Yamashita T, Ito H. Appl Phys Lett 2001;79:1079.
19. Shoji S, Kawata S. Appl Phys Lett 1999;75:737.
20. Zupan M, Deshpande VS, Fleck NA. Eur J Mech A 2004;23:411.
21. Deshpande VS, Fleck NA. Int J Solid Struct 2001;38:6275.
22. Gere JM, Timoshenko SP. Mechanics of materials. Monterey, CA: Wadsworth; 1984.